Synthesis of CVD Diamond nanoparticles and Cytotoxicity evaluation in murine metastatic melanoma cells

Cristiane Costa Wachesk (cris_cw@hotmail.com)
Universidade Federal de Sao Paulo https://orcid.org/0000-0003-4786-401X
Carolina Guimarães Hurtado
Universidade Federal de Sao Paulo
Rebeca Falcão
Universidade Federal de Sao Paulo
Dayane Batista Tada
Universidade Federal de Sao Paulo
Getulio Vasconcelos
Instituto de Estudos Avancados
Evaldo José Corat
Instituto Nacional de Pesquisas Espaciais
Vladimir Jesus Trava Airoldi
Instituto Nacional de Pesquisas Espaciais

Research

Keywords: HFCVD diamond, Laser Ablation, CVD Diamond Nanoparticles (CVD-DNPs), Drug Delivery, Melanoma

Posted Date: February 12th, 2020

DOI: https://doi.org/10.21203/rs.2.23254/v1

Synthesis of CVD Diamond nanoparticles and Cytotoxicity evaluation in murine metastatic melanoma cells

Cristiane da Costa Wachesk[1,4*], Carolina Ramos Hurtado[1,2], Rebeca Falcão Borja de Oliveira Correia[1,4], Dayane Batista Tada[1], Getúlio Vasconcelos[3], Evaldo José Corat[4], Vladimir Jesus Trava-Airoldi[4]

[1] *Laboratory of Nanomaterials and Nanotoxicology - Institute of Science and Technology, Federal University of São Paulo (UNIFESP), Talim Street, 330 - Vila Nair, São José dos Campos – SP, Brazil, 12231-280*

[2] *Federal Institute of São Paulo (IFSP), Rod. Pres. Dutra, km 145 - Jardim Diamante, São José dos Campos - SP, 12223-201*

[3]*Laboratory of Lasers and Optical Applications Development - Dedalo, Institute of Advanced Studies (IEAv), Coronel Aviador José Alberto Albano do Amarante, 01 - Putim, São José dos Campos - SP, Brazil, 12228-001*

[4]*Associated Laboratory of Sensors and Materials - National Institute for Space Research (INPE) – Astronautas Avenue, 1.758 - Jardim da Granja, São José dos Campos – SP, Brazil, 12227-010*

*Corresponding author: Cristiane da Costa Wachesk

Tel.: +55 12 981247203

Fax: +55 12 32086558

E-mail: **cris_cw@hotmail.com**

Abstract

Diamond nanoparticles (DNPs) have showed *in vitro* and *in vivo* biomedical applicability due to their low toxicity and biocompatibility. Recent studies have focused on the potential use of (DNPs) as suitable vehicles for improving drug delivery in cancer treatment. The advantages of DNPs lies in their high stability and small size compared to other carbon-based nanomaterials. In this work, CVD-diamond nanoparticles (CVD-DNPs) were synthesized and evaluated regarding their application as a new drug delivery platform for metastatic melanoma therapy. A new synthesis technique developed DNPs from CVD diamond thin film. This type of diamond has the same physical and chemical properties as a natural diamond: extreme hardness, excellent thermal conductivity, low coefficient of friction, biocompatibility, chemically inert for temperatures below 800^0 C, among others. The main objective of this study was to produce CVD-DNPs by laser ablation and to evaluate their cytotoxicity. A pulsed, ytterbium-doped fiber (Yb) was used to form DNPs in the pure aqueous medium (Milli-Q). The final suspension was obtained at high concentration of the CVD-DNPs and it was used to evaluate the cytotxicity in murine metastatic melanoma B16-F10 cells by using colorimetric assays. The characterization by FT-IR, X-Ray, DLS, RAMAN, SEM, and TEM demonstrated the successful synthesis of CVD-DNPs with a hydrodynamic diameter of 57 and 54 nm. *In vitr*o studies performed for 24h and 48h resulted in viability of 70-80% of cells incubated with CVD-DNPs at 250 μg/mL, which demonstrated a insignificant cytotoxic effect. Thus, these results suggest a potential use of CVD-DNPs as a drug delivery platform for antitumoral therapy.

Keywords: HFCVD diamond, Laser Ablation, CVD Diamond Nanoparticles (CVD-DNPs), Drug Delivery, Melanoma.

1. **Introduction**

Diamond has a diversity of extraordinary properties that continue to attract scientific interest in the search for new technological applications [1], [2], [3]. This widespread interest has led to new approaches for the growth and processing of diamonds and diamond films [4]. A series of applications have been developed based on the combination of diamond properties and the multiplicity of film properties obtained by combining the microstructure, morphological surface, impurities and surfaces [4], [5].

Diamond Nanoparticles (DNPs) are a class of carbon-based nanomaterials of increasing interest in science and technology [3], including their use as a drug delivery [4]. DNPs are inert [5], optically transparent, photo-luminescent [6] and biocompatible [7]. The application of DNPs as drug delivery platform for cancer therapy is based on the passive tumor targeting due to the enhanced permeability and retention (EPR) effect known for NPs of 30-100 nm. Also, the efficiency of DNPs as drug delivery has been proved to be a result of increased vascular permeability provided by DNPs [4] [8]. Additionally, DNPs have been shown to remain inside the cell for a longer period of time, increasing the efficiency of chemotherapeutic treatment. These effects have been pointed to be a result of the cell internalization of DNPs by endocytosis [8] and which may eventually carry also external compounds into the cell due their complexation with DNPs [9]. Since DNPs can bind tightly to a variety of molecules and deliver them directly to a tumor [10], the use of DNPs as delivery agents considerably reduces the toxic side effects of chemotherapy [11]. Therefore, DNPs are a useful tool in the search for ~~a~~ better drug administration against cancer via an induced permeability of vascular barrier [3], [13].

As with all commercial applications, cost-efficient production methods are as important as the application itself. Current research has focused on how DNPs can be synthesized through explosions. More recent studies show that the synthesis of detonation DNPs has already been optimized for a commercial scale, with rigid structure clusters that can reach hundreds of nanometers or even several micrometers [13]. Therefore, for most of its applications, particularly in biology and medicine, DNPs must be purified after synthesis[14]. There are other ways for synthesizing NPs which may be classified in two approaches: “bottom-up”, when atoms are aggregated to originate the nanomaterial and “top-down”, when the material is removed from a

bulk structure [15],[16].–Pulsed laser ablation used in this study is a top-down approach which is gaining special attention within the scientific community [17],[18],[19].

This study was focused in producing low-cost CVD-Diamond Nanoparticles (CVD-DNPs) and in studying their cytotoxicity in order to evaluate a possible application as drug delivery platform. In order to synthesize CVD-DNPs it was used a Synthetic CVD-diamond obtained by an innovative technology manufacturing from CVDVale company. The CVDVale uses hot-filament chemical vapor deposition (HFCVD), which makes the CVD diamonds suitable for implantable medical, dental and drug delivery interests. This work addresses the use of LASER ablation and evaluate the impact of this technique on the particle size, morphology and cytotoxicity of CVD-DNPs.

Materials and methods

2.1 CVD Diamond Productions

For diamond film growth, the an HFCVD reactor was used, composed of a set of 6 tungsten filaments with diameters of 125µm, equidistant by 4 mm, maintained at a temperature of approximately 2200 ° C. The total gas pressure was of 50 Torr during the 3h of growth. The reactive gas mixture consisted of 2% CH4 and 98% H2. The ramp downturn off period was of 1 h. The sample was placed on the substrate holder at a distance of 5 mm for growth at 700ºC, was approximately 0.43 µm/h and 10 mm for growth at 550ºC. The about 30 to 50 micrometer microcrystalline diamond was grown in columnar structure without re-nucleation This is used process in CVDVale that is a company specialized on the CVD-diamond coating.

2.2 Synthesis and Preparation of the CVD Nano-diamond Suspensions

In order to perform the laser ablation process, we used CVD-diamond film obtained via the HFCVD technique provided from CVD Vale Company. CVD diamond film 30 µm thick was macerated using an agate mortar and pestle, and sifted in a granulometry sieve of 200 mesh (0.074 mm of mesh opening). CVD-diamond 5mg/mL aqueous suspensions from Deionizer Millipore Milli-Q system (40mL volume) were prepared and irradiated by pulsed laser ablation of ytterbium-doped fiber (Yb) (λ=1062nm) using the PRO Marking (Pulsed Fiber-Yb laser), as shown in (Fig. 1), the CVD-DNPs were ablated, at 30 (i) and 60 (ii) min time. Next, the colloidal suspension was centrifuged in Hettich Rotina 4500RPM for 0 and 60 min respectively, to remove aggregates,

shown in Table 1. After for the purpose of removing of organic contaminants was used hydrofluoric acid (HF) for the removal of SiO2 from contamination of the sample by abrasion of the Agate mortar. In order to reduce the size of CVD-NDs, at 30 (i) and 60 (ii) min time, the colloidal suspensions was centrifuged for 0 and 60 min respectively, as shown in Table 1.

The CVD-DNPs were obtained by the laser ablation method. Using a gaussian laser beam, pulsed average power 20 W, pulse time of 200 ns and frequency of 45 (KHz) the irradiance is obtained by:

$$I\left({}^{W}/_{cm^2}\right) = \frac{2.P_{k(W)}}{\pi.r^2} \quad ; \tag{1}$$

Where,

$$P_{k=}\frac{P_M}{f(H_z).t_p(s)} \tag{2}$$

and where the minimum beam Ø is 0.04 mm, obtained by:

$$W_{min} = \frac{\lambda.f}{\pi.w_0} \quad ; \tag{3}$$

Where,

$\lambda = 1064\ nm\ ((beam\ length))$,

$f = 190\ nm\ (focal\ distance)$, and where

$w_0 = 10\ mm\ (beam\ diameter$ "in");

Which results in:

$$I\left({}^{W}/_{cm^2}\right) \sim 10^9\ \left({}^{W}/_{cm^2}\right) \tag{4}.$$

However, considering that this beam radiated particles of 10 micrometers of edge during the experiment, it is reasonable to consider that these microparticles when irradiated in the highest energy region of the beam (central region) are ablated.

2.3 Characterization techniques

2.3.1 Dynamic Light Scattering (DLS) and Zeta Potential

Hydrodynamic diameter, size distribution and ζ-potential values were obtained through the dynamic light scattering (DLS) technique. The equipment used for this analysis was the DelsaTM Nano C by Beckman Coulter, belonging to ICT-UNIFESP multi-user NAPCEM laboratory. For each sample, the dilutions were made in deionized water and the measurements were performed in triplicate to obtain mean and standard deviation values, both generated by the equipment software.

2.5 Raman Scattering Spectroscopy

The Raman scattering spectra were obtained using the Horiba Scientific equipment with a helium cadmium laser excitation (325 nm), from LAS/INPE. It is a vibrational spectroscopy technique used for molecular structures determination, quantification, materials identification and the degree of crystalline network disorder information. Raman spectroscopy was also used to identify different forms of carbon.

2.3.2 X-Ray diffractometry

The diffractograms were obtained using the PANalytical brand system from the X'PertPro series, from LAS-INPE and operated at 45kV and 40mA. This technique was used to identify and quantify crystalline phases, orient crystallites, determine single cell parameters and residual stress [20] .

2.3.4 FT-IR (Fourier Transformed Infrared Spectroscopy)

The infrared spectra were acquired by Fourier transform infrared spectroscopy using a universal attenuated total reflectance sensor (FT-IR-UATR) (Perkim Elmer Spectrum, model Frontier). The FT-IR spectrum was an average of 32 scans at a speed of 2s per scan in a range of 400-4000cm^{-1}. The resolution of the spectrometer was of 4cm^{-1}.

2.3.5 Field Emission Scanning Electron Microscopy (SEM-FEG)

CVD-DNPs were physically and morphologically characterized using the scanning electron microscope. The micrographs were performed in collaboration with the LAS/INPE group and obtained with Field Emission Scanning Electron Microscopy by Tescan Mira 3, MIRA 3 model; which was coupled to the X-Ray dispersive energy spectroscopy (EDS) system.

2.3.6 Transmission Electron Microscopy (TEM)

The micrographs were obtained using the Transmission Electron Microscope MET Tecnai G2 Spirit BioTWIN 120 kV (FEI) through a digitally controlled system, CompuStage Single-Tilt tilt support, Olympus-SIS Veleta CCD 120/200 kV digital camera, tungsten emitter (W), TIA (TEM Imaging and Analysis) program for image visualization, in collaboration with the Institute of Advanced Studies of the Sea (IEAMar), UNESP.

2.4 In vitro assays

2.4.1 Cell culture and cell line

The cell line studied here as a tumor cell model was B16F10-Nex2 cells kindly provided by Laboratory of experimental biology of cancer (LABEC-UMC, BR). Tumor line B16 was isolated from spontaneous melanoma in C57Bl / 6 animals. Fidler [21] obtained gradually more aggressive and invasive strains after successive in vivo passages, numbering them from F1 to F10. The most aggressive strain was B16F10, obtained from the Ludwig Institute for Cancer Research. B16F10-Nex2 cells were maintained at 5% CO2 at 37°C and grown in medium RPMI-1640 (GIBCO) composed of vitamins, amino acids, salts, D-glucose, 24 mM sodium bicarbonate, 40 mg / mL gentamicin (GIBCO) and supplemented with 10% fetal bovine serum (SFB) (Cultilab), pH 7.4. For cell washing, the buffer was used. PBS (Phosphate Buffer Saline). Composition: 140 mM de NaCl, 2,7 mM, KCl, 10 mM de Na_2HPO_4, 1,8 mM KH2PO4, pH 7,4). Since B16F10-Nex2 cells are adherent, trypsin (GIBCO) was used to release cells from culture flasks and plates.

2.4.2 Analysis of cell viability

The cell viability assay was based on the indirect measurement of mitochondrial activity of cells after incubation with the materials under study. In viable cells, the salt 3-[(4,5-dimethylthiazol-2-yl)-2,5-diphenyltetrazolium bromide] (MTT) (Sigma-Aldrich) is reduced and forms formazan, which is a purple insoluble salt. The formazan is quantified by absorbance measurement after solubilization in organic solvent. So, in this study, B16 cells were cultivated in RPMI1640 culture medium and plated in 96-well plates at the concentration of 10^3 cells per well (300 µL). After 12h, the supernatant was removed and the cells were incubated with 50 µL of 5 different

concentrations of CVD-DNPs suspension. Then, after the incubation period of 24 and 48h, the culture medium was removed and 100 µL of MTT solution (2mg/mL, PBS solvent) was added in each well. The MTT was removed 3h later and the formazan salt was solubilized with 200 µL of DMSO. The solution was left to rest for 30 min, followed by measurement of absorbance at 540nm at the plate reader (Biotek). Absorbance of the wells wherein the cells were incubated in the absence of NDs were considered as 100 % of viability.

2.4.3 Statistical Analysis

The assays were performed in quintuplet, expressed as mean ± standard deviation and mean ± mean standard error of MTT assays. All the assays were statistically analyzed by Graphpad Prism® software, using the one way analysis of variance (ANOVA), followed by the Bonferroni test in order to compare with the control group. A probability value equal or less than 0.05 was considered statistically significant.

3. Results and discussion

The relationship between the morphology of diamond crystals and the conditions of their crystallization has been the subject of great scientific debate in the last two centuries. Based on the analysis of external morphology and diamond surface. The according to Evdokimov [22] concluded that more than one growth and dissolution process can occur in the same crystal, revealing precisely the same surface shapes, and may represent overlapping stages of growth and/ or dissolution. In our diamonds, the symmetry of their structure was demonstrated by the material's morphology from SEM-FEG analysis, where one may note the faceted morphology of the CVD Diamond crystals (Fig. 2). Particles irradiated by the beam in area 1 are heated, in area 2 are ablated and consequently the size reduction, as shown in the (Fig. 3).

Water suspensions of laser ablation CVD-DNPs, were used to determine the obtained particle size distribution through the centrifugation process at 4500 rpm, performed at different times of 0 and 60min (Table 2).

A decrease in particle size was observed (Fig. 4). The results show a reduction in particle size due to the laser ablation and centrifuging time where it occurred the disagglomeration and stability of CVD-DNPs. This size is very close to the size of a single diamond nanocrystallite [23]. This can be seen by the left dislocating curves at 30-60 min ablation time and 0-60 min centrifugation time,

where the medium hydrodynamic radius was 54 and 57nm (Fig. 4a-b); while in the non-centrifuged CVD-DNPs , the medium was 72 and 82 nm (Fig. 4c-d), respectively. Furthermore, a wider distribution curve is shown with laser ablation time and centrifugation for 60 minutes, provided the precipitation of bigger nanoparticles and the average diameter of NDs in suspension.

The high stability of aqueous suspension of CVD-DNPs was indicated by the low polydispersity index (PI) (0.2) and a small increase in the mean value of hydrodynamic diameter during the observed period. The high stability was provided by the high charge density on the NDs surface as suggested by the high value of Zeta-potential (-36.39 and -30.94 mV) respectively (Table 3).

According to studies by Koniakhin [24], these values of z-potential exhibit the evidence of the produced colloidal stability. Measures were taken in colloidal solutions before and after centrifugation. From the measurements carried out on these solutions, a comparison between the results of the mean hydrodynamic size measurements using SEM and TEM analysis was possible. A purpose of purity identification and contaminant ND content were used to characterize the characteristics used SEM / TEM [25] , XRD [26] Raman Spectroscopy [27]and FTIR [28].

Figure 5 shows images after laser ablation for 60 min and after centrifugation for 60 min, respectively. There was a morphological change in the diamonds, due to the process (Fig. 5 a). Based on the obtained images, it was possible to visualize the aggregates of CVD formation and also the uniformity in particle size. In addition, the ablated and centrifuged CVD-DNPs are significantly smaller in size. The images made in SEM-FEG were analyzed with the software imageJ. Using the software, it is possible to measure the size of CVD-DNPs made in SEM-FEG by taking a statistical count to find the mean size value of the size distribution for each sample. For each case, using a sample of 100 particles, we obtained the particle size distribution curve, as shown in Figure 5 b. The average particle size of the CVD-NDs for before and after centrifugation was 50.62 ± 14.28 nm.

Figure 6 shows the average particle size, morphology and dispersion of CVD-DNPs after ablation as obtained by transmission electron microscopy (TEM), after centrifugation (Fig. 6a). Note there was a morphological difference. The synthesized CVD-DNPs are agglomerated with rounded shape due to the performed process. Figure (6b) shows the image analyzed with the imageJ software to

estimate size distribution. Thus, four regions of each sample were analyzed; that is, a statistical calculation was done by adding the areas of the CVD-DNPs found in each of the two images taken for each sample. The medium particle size for the samples after centrifugation and laser ablation was 20.50 ± 6.19 nm. In addition, the discrete difference evidenced by the Dynamic Light Scattering (DLS) and the Scanning Electron Microscopy (SEM) in relation to the NDs size, does not characterize the results found as incompatible, since the second method provides only a small portion of the nanoparticles isolated from the medium. In the case of transmission electron microscopy (TEM), the diameters found were between 10 and 20 nm. According to the results, laser ablation time and the centrifugation process produces with diamond nanoparticles having the size of nanometric [29].

From the dispersive energy spectroscopy (EDX), it was possible to analyze the chemical composition of the CVD-DNPs before and after the laser ablation and centrifugation processes. For this analysis, a drop of the colloidal solution was placed under a carbon tape. Due to equipment limitations, we chose a sample region of EDS with larger particles (Fig. 7). EDX spectrum with 5kV energy from laser ablation sample (Fig. 10a) shows the mass concentration, where we obtained the same 97.1% carbon and 2.9% oxygen values; (Fig. 7b) shows the mass concentration, where we obtained the same 77.8% carbon and 22.2% oxygen values; and (Fig. 7 c) shows the mass concentration, where we obtained the same 78.3% carbon and 21.7% oxygen values, thus Indicating that carbon is present in these samples. Oxygen concentration is possibly due to high reactivity; in both CVD-DNPs groups the concentration remained the same. According to Pearce [29] EDX spectra indicated the presence of only C and O; the purified NDs also confirmed the absence of impurities. This result supports those of Yang et al. [30], and confirms that diamond may be produced by ablation ~~of~~ under water. Results indicate that, as expected, the final material does not present contamination in the CVD-DNPs from the ablation techniques.

The Raman spectra of all ND colloids suspensions after the laser ablated CVD-DNPs processing, were measured using a laser Raman spectrometer using 25% of laser power with wavelength of λ = 532nm (Fig. 8). The material was characterized by Raman spectroscopy, which provides the information of photoluminescence frequency of different carbon structures [31], The size of the nanodiamonds was also studied using Raman spectroscopy. From the Raman spectroscopy analysis, it is possible to determine molecular structures, quantify and identify materials and

degree of crystalline network disorder. The spectral analysis of the CVD-diamond sample showed the characteristic peak of sp3 hybridization at 1332 cm [32] of a residual stressless diamond [33] (Fig. 8a). The band of amorphous carbon, centered at 1550 cm $^{-1}$, much wider than diamond, was also observed. The peaks found for all CVD-diamond samples and CVD-DNPs analyzed, confirm the literature data that point out the Raman shift at 1332.5 (cm-1) for carbon in the formation of crystalline diamond, is at 1550 (cm-1) for amorphous carbon [34]. The evident luminescent background is due to its visible luminescence spectrum, as well as to the symmetry of the carbon atoms in the form of graphite (sp2 hybridization) on the CVD-diamond crystal and to the continuous emission as a result of expected crystal defects in CVD-diamond. Due to the laser ablation process, it was possible to reduce the diamond crystals' size and their luminescence effect in the Raman spectrum, Fig 8b-c respectively, characteristic of structural diamonds.

Another feature to be emphasized is the principle of incident and dispersed light, where the intensity of the Raman lines is dramatically increased when the scattered light intensity, between the incident photon**s** is equal to the permissible electronic interband transition energy [34],[35],[36],[37]. The In both spectra, there was a high degree of purity of the diamond, due to the low G-band intensity which is related to a low graphite inclusion in the diamond, proving the technological efficiency of the process. Therefore, the laser ablation process showed no difference, indicating that the resulting material was not modified.

To identify the contamination present in CVD diamond films and CVD-DNPs, a detailed FTIR analysis was performed on each sample as well as the used in laser ablation synthesis. Thus it was possible to verify whether there were changes in the chemical structure resulting from ablation.
since it will provide the possibility of functionalization of NDs surface in order to promote biological or materials application.

The FT-IR spectra of the CVD-Diamond sample and the CVD-DNPs obtained herein are depicted in (Fig. 9). The spectra are presented in a range between 4000 and 400cm $^{-1}$. Above 4000cm^{-1} there ~~is~~ was no absorption in any of the samples. On the other hand, with the ATR sampling technique used, the absorbances obtained below 400cm^{-1} were no longer reliable. Spectrum analysis was performed based on the peak assignment available in the literature [38]**.** The absence of absorption bands in the FT-IR spectrum of CVD diamond confirmed that this sample did not have

to contamination (Fig. 9a). The FT-IR spectrum of CVD-DNP laser ablation (Fig. 9 b-c) showed a very intense band at 1089 cm-1 and 777 cm-1, which were attributed to Si-O-Si stretching and bending, suggesting the contamination of the sample with silica due to contamination with agate mortar and pestle, wherein the raw diamond was macerated at the beginning of the process of NDs preparation.Despite the contamination with Si-O-Si silica, FT-IR spectrum indicated that NDs obtained herein starting from laser ablation could be eliminated by acid treatment with HF followed by washing with deionized water and centrifugado for 300 min time. The successfulness of cleaning step could be certified by the absence of Si-O-Si silica absorption band in the FT-IR spectra of cleaned CVD-DNPs obtained herein are depicted in (Fig. 9 d-e).

Based on the identification and quantification of crystalline phases, the determination of single cell parameters, the orientation of crystallite, and, finally, the determination of residual stress [39] and its possible contaminants, we used an X-Ray diffractometer the identification and quantification of crystalline phases. The material was characterized by x-ray diffraction before and after laser ablation (Figure 10), using the Highscore software. From these results we can observe the characteristic diffraction peaks of the diamond, for angles of 2Θ = 43, 9º, 75,3º and 91,5º, concerning the diffraction of the planes (111), (220) and (311), respectively as shown in (Fig. 10 a), with Plane (111) being the most intense. From this analysis it was verified that the CVD-DNPs did not present any contamination after laser ablation and CVD-DNPs purification process.

Using the Scherrer equation [40], [37], [41], and the values of the width at half height of the most intense diamond, considering λ=1.54056, it was possible to calculate the crystallite size (Eq.1):

$$D = \frac{k\lambda}{\beta \cos \theta} \quad ; \tag{5}$$

Where,

D = average size of the crystallite,

k = dimensionless form factor,

β = line widening in radians,

θ = Bragg angle, and

λ = X-ray wavelength.

The mean size was determined from the total half-width maximum (FWHM) of the X-ray diffraction peak [42].

The FWHM value includes errors originating from noise and equipment conditions, such as the width of the X-ray diffraction slit. In general, it is difficult to calculate the deconvolutions when the observed signals have high level noise. According to table 4, to obtain the FWHM value of each peak, we used the Voigt line shape approximation by the sum of a Gaussian-type distribution and a Lorentzian width [43] .

It is clear that, sample ablated for 60 minutes has a wider peak,as shown in Table 4 for all diffraction planes showing a smaller particle size.Likewise, (Fig. 10 b-c) shows the orientation of crystallite (111) in the characterization of CVD Diamond after the laser ablation process, the Fig. (10 d-e) shows that the purification process was efficient for cleaning the CVD-DNPs. In accordance with theoretical studies reported by Telling [44], the Diamond cleavage energy was lower for Plane (111), meaning that there was a priority for the cleavage of the CVD diamond in these crystalline phases. The experimental results presented are coherent with the literature. All observed peaks are in accordance with JCPDS (Joint Committe e on Powder Diffraction Standards) no. 00-006-0675 (ND).

Considering that one of the main applications of DNPs under investigation in biomedical field has been as drug delivery for cancer therapy [45][46], we evaluated the cytotoxicity of the DNPs prepared herein. With this purpose, the MTT assay was used, which offers a quantitative, convenient method for evaluating whether a material affects cell viability. The extension of MTT reduction by mitochondria of viable cells is proportional to the absorbance of formazan [47]. CVD-DNPs, cytotoxicity was evaluated against murine melanoma cells B16F10. MTT assay was performed by incubating cells during 24h and 48h with CVD-NDs at 5 different concentrations: CVD-DNPs (0.05 μg/mL), (25 μg/mL), (50 μg/mL), (125 μg/mL), (250 μg/mL). As depicted in Figure 11, CVD-DNPs were not cytotoxic to B16 cells after 24h of incubation at any of the studied concentrations. In this assay, all the values of cell viability were equal or above 70%, considered the standard deviation, which is a limit value accepted to consider a material as non-cytotoxic. This observation is in agreement with the results reported by Schrand et al. [48]. In their work, NDs of

2–10 nm of diameter were not cytotoxic to neuroblastoma cells nor to macrophages at concentrations in the range of 5-100 μg/mL.

Nevertheless, CVD-DNPs showed increased cytotoxicity after 48h of incubation. At the range of 0.05-125 μg/mL cell viability decreased in function of CVD-DNPs concentration. Interestingly, at the highest concentration of 250 μg/mL, the cell viability was high (76%), indicating non-cytotoxicity at this condition. Although the increased cytotoxicity after longer time of incubation was not observed by Gismondi et al. [46] after incubation of B16 and HeLa cells with NDs, the authors used smaller DNPs (4-5 nm) and a higher concentration range (5-200 μg/mL). Our results were in line with previous observations of the group and with the information found in the literature [49][50][51]. The cytotoxicity of CVD-DNPs at low concentration is a consequence of the interaction between small nanoparticles with cell membrane, inducing loss of membrane integrity and cell death. On the other hand, when CVD-DNPs are at higher concentration, they are prone to form big aggregates, mainly due to the proteins of the culture medium, which adsorb on ND surfaces. These bigger structures are not able to insert into cell membrane and therefore the cell viability is not compromised. Therefore, once the low cytotoxicity is one of the key features required for a drug delivery platform [48], the NDs prepared in this work have the potential to be used in the therapy of cancer, as for example of melanoma. Notably, the concentration of DNPs suspension has to be carefully controlled. Another alternative is the application of these small DNPs to prepare bigger structures wherein several kinds of drugs could be loaded, as already reported [46] [48].

4. Conclusion

The synthetic diamond-CVD, which has the same physical and chemical properties as natural diamonds, was useful to synthesize DNPs by Laser ablation (ytterbium doped fiber laser). It was possible to obtain DNPs with average hydrodynamic diameter of 54 nm and a particle size distribution between -2-10 nm. These CVD-DNPs properties favor the adsorption or complexation with other compounds, and the cell internalization due to their small size. The cost of diamonds is getting smaller and smaller, encouraging the use of this important class of materials for a variety of applications, especially biological ones. The cell viability assay showed low cytotoxic of CVD-

DNPs. The incubation of murine metastatic melanoma B16-F10 cells with CVD-DNPs for 24h and 48h resulted in cell viability of 70-80% at 250 μg/mL. The low cytotoxicity against tumor cells indicated the potential use of CVD-DNPs as drug delivery platforms for antitumoral therapy. The conjugation of photosensitizers (PS) CVD- DNPs, and cytolocation will be investigated in future stages of this research.

6. Declarations

6.1 Ethics approval and consent to participate
Not applicable.

6.2 Consent for publication
Not applicable.

6.3 Availability of data and material
All data generated or analyzed during this study are included in this published article.

6.4 Competing interests
The authors declare that there is no conflict of interest.

6.5 Funding
FAPESP (grant number 2012/15857-1; 2017/01697-6), National Council for Scientific and Technological Development (CNPq) (grant number 380402/2019-0) Coordination for the Improvement of Higher Education Personnel (*CAPES*) , The funding was provided by Fundação de Amparo à Pesquisa do Estado de São Paulo (Grant Nos. 2017/01697-6 and 2012/15857-1).

6.6 Authors' contributions
All authors were involved in writing the manuscript. All authors contributed to the experimental design. All authors read and approved the final manuscript.

6.7 Authors' information
Affiliations

1. Nanomaterials and Nanotoxicology Laboratory, Institute of Science and Technology, Federal University of São Paulo (UNIFESP), Talim, 330 – Vila Nair, São José dos Campos, São Paulo, 12231-280, Brazil.
Cristiane da Costa Wachesk,
Carolina Ramos Hurtado,Rebeca Falcão Borja de Oliveira Correia,
& Dayane Batista Tada

2. Federal Institute of São Paulo (IFSP), Rod. Pres. Dutra, km 145 - Jardim Diamante, São José dos Campos, São Paulo, 12223-201, Brazil.

Carolina Ramos Hurtado

3. Laboratory of Lasers and Optical Applications Development - Dedalo, Institute of Advanced Studies (IEAv), Coronel Aviador José Alberto Albano do Amarante, 01 - Putim, São José dos Campos, São Paulo,12228-001, Brazil.
Getúlio Vasconcelos

4. Sensors and Materials Associated Laboratory, National Institute for Space Research (INPE), Av. dos Astronautas, 1.758 - Jardim da Granja, São José dos Campos, São Paulo, 12227-010, Brazil.
Cristiane da Costa Wachesk,
Rebeca Falcão Borja de Oliveira Correia,
José Evaldo Corat,
& Vladimir Jesus Trava-Airoldi

6.8 Acknowledgements

The authors want to acknowledge support from Institute for Advanced Sea Studies (IEAMar/UNESP) and Brazilian National Council for Scientific and Technological (CNPq). Ministry of Science, Technology and Innovation (MCTI) and the PRO marking company, for the use of ytterbium doped pulsed fiber laser.

Corresponding author
Correspondence to Cristiane da Costa Wachesk.

7. References

[1] May P W 1995 CVD diamond: a new technology for the future? 101–6
[2] Nemanich R J, Carlisle J A, Hirata A and Haenen K 2014 CVD diamond - Research, applications, and challenges *MRS Bulletin* **39** 490–4
[3] Engineering B, Cha C, Shin S R, Annabi N and Dokmeci M R Carbon-Based Nanomaterials : Multifunctional Materials for
[4] Ansari S A, Satar R, Jafri M A, Rasool M, Ahmad W and Kashif Zaidi S 2016 Role of Nanodiamonds in Drug Delivery and Stem Cell Therapy *Iranian Journal of Biotechnology* **14** 130–41
[5] Holt K B 2007 Diamond at the nanoscale: Applications of diamond nanoparticles from cellular biomarkers to quantum computing *Philosophical Transactions of the Royal Society A: Mathematical, Physical and Engineering Sciences* **365** 2845–61
[6] Mona J, Tu J S, Kang T Y, Tsai C Y, Perevedentseva E and Cheng C L 2012 Surface modification of nanodiamond: Photoluminescence and Raman Studies *Diamond and Related Materials* **24** 134–8
[7] Xing Y and Dai L 2009 Nanodiamonds for nanomedicine *Nanomedicine* **4** 207–18
[8] Verma A, Uzun O, Hu Y, Hu Y, Han H S, Watson N, Chen S, Irvine D J and Stellacci F 2008 Surface-structure-regulated cell-membrane penetration by monolayer-protected nanoparticles *Nature Materials* **7** 588–95

[9] Setyawati M I, Mochalin V N and Leong D T 2016 Tuning endothelial permeability with functionalized nanodiamonds *ACS Nano* **10** 1170–81
[10] El-say K M 2011 <El-Say, 2011.pdf> **01** 29–39
[11] Li J, Zhu Y, Li W, Zhang X, Peng Y and Huang Q 2010 Nanodiamonds as intracellular transporters of chemotherapeutic drug *Biomaterials* **31** 8410–8
[12] Wu M S, Sun D S, Lin Y C, Cheng C L, Hung S C, Chen P K, Yang J H and Chang H H 2015 Nanodiamonds protect skin from ultraviolet B-induced damage in mice *Journal of Nanobiotechnology* **13** 1–12
[13] Krueger A 2008 Diamond nanoparticles: Jewels for chemistry and physics *Advanced Materials* **20** 2445–9
[14] Turcheniuk K and Mochalin V N 2017 Biomedical applications of nanodiamond (Review) *Nanotechnology* **28** 252001
[15] Zeng H, Du X W, Singh S C, Kulinich S A, Yang S, He J and Cai W 2012 Nanomaterials via laser ablation/irradiation in liquid: A review *Advanced Functional Materials* **22** 1333–53
[16] Amendola V and Meneghetti M 2013 What controls the composition and the structure of nanomaterials generated by laser ablation in liquid solution? *Physical Chemistry Chemical Physics* **15** 3027–46
[17] Tan D, Lin G, Liu Y, Teng Y, Zhuang Y, Zhu B, Zhao Q and Qiu J 2011 Synthesis of nanocrystalline cubic zirconia using femtosecond laser ablation *Journal of Nanoparticle Research* **13** 1183–90
[18] Tan D, Xu B, Chen P, Dai Y, Zhou S, Ma G and Qiu J 2012 One-pot synthesis of luminescent hydrophilic silicon nanocrystals *RSC Advances* **2** 8254–7
[19] Tan D, Zhou S, Xu B, Chen P, Shimotsuma Y, Miura K and Qiu J 2013 Simple synthesis of ultra-small nanodiamonds with tunable size and photoluminescence *Carbon* **62** 374–81
[20] Kvick A 2016 X-Ray Diffraction, Materials Science Applications *Encyclopedia of Spectroscopy and Spectrometry* 648–55
[21] Fidler I J 1975 Biological Behavior of Malignant Melanoma Cells Correlated to Their Survival in Vivo *Cancer Research* **35** 218–24
[22] Evdokimov M D, Ladygina M Y and Nesterov A R 2001 Morphology of diamonds as a possible indicator of their genesis *Neues Jahrbuch fur Mineralogie, Abhandlungen* **176** 153–77
[23] Dideikin A T, Aleksenskii A E, Baidakova M V., Brunkov P N, Brzhezinskaya M, Davydov V Y, Levitskii V S, Kidalov S V., Kukushkina Y A, Kirilenko D A, Shnitov V V., Shvidchenko A V., Senkovskiy B, Shestakov M S and Vul A Y 2017 Rehybridization of carbon on facets of detonation diamond nanocrystals and forming hydrosols of individual particles *Carbon* **122** 737–45
[24] Koniakhin S V., Besedina N A, Kirilenko D A, Shvidchenko A V. and Eidelman E D 2018 Ultracentrifugation for ultrafine nanodiamond fractionation *Superlattices and Microstructures* **113** 204–12
[25] Shames A I, Panich A M, Kempiński W, Alexenskii A E, Baidakova M V., Dideikin A T, Osipov V Y, Siklitski V I, Osawa E, Ozawa M and Vul' A Y 2002 Defects and impurities in nanodiamonds: EPR, NMR and TEM study *Journal of Physics and Chemistry of Solids* **63** 1993–2001
[26] Costa G C C, Shenderova O, Mochalin V, Gogotsi Y and Navrotsky A 2014 Thermochemistry of nanodiamond terminated by oxygen containing functional groups *Carbon* **80** 544–50
[27] Mermoux M, Crisci A, Petit T, Girard H A and Arnault J C 2014 Surface modifications of detonation nanodiamonds probed by multiwavelength raman spectroscopy *Journal of Physical Chemistry C* **118** 23415–25

[28] Petit T and Puskar L 2018 FTIR spectroscopy of nanodiamonds: Methods and interpretation *Diamond and Related Materials* **89** 52–66
[29] Pearce S R J, Henley S J, Claeyssens F, May P W, Hallam K R, Smith J A and Rosser K N 2004 Production of nanocrystalline diamond by laser ablation at the solid y liquid interface **13** 661–5
[30] Nistor L C and Epurescu G 1998 Preparation of nano-crystalline diamonds using pulsed laser induced reactive quenching Preparation of nano-crystalline diamonds using pulsed laser induced reactive quenching
[31] Ferrari A C and Robertson J 2004 Raman spectroscopy of amorphous, nanostructured, diamond-like carbon, and nanodiamond *Philosophical Transactions of the Royal Society A: Mathematical, Physical and Engineering Sciences* **362** 2477–512
[32] Ager J W and Drory M D 1993 Quantitative measurement of residual biaxial stress by Raman spectroscopy in diamond grown on a Ti alloy by chemical vapor deposition *Physical Review B* **48** 2601–7
[33] Michler J, Mermoux M, Von Kaenel Y, Haouni A, Lucazeau G and Blank E 1999 Residual stress in diamond films: Origins and modelling *Thin Solid Films* **357** 189–201
[34] Knight D S and White W B 1989 Characterization of diamond films by Raman spectroscopy **16802** 385–93
[35] Moskovits M 2005 Surface-enhanced Raman spectroscopy: A brief retrospective *Journal of Raman Spectroscopy* **36** 485–96
[36] Kneipp K, Kneipp H, Itzkan I, Dasari R R and Feld M S 2002 Ultrasensitive Chemical Analysis by Raman Spectroscopy *Chemical Reviews* **99** 2957–76
[37] Determination P S 1939 No Title **56** 978–82
[38] Dischler B, Wild C and Koidl P 1993 *Hydrogen in polycrystalline diamond* vol 185 (ELSEVIER B.V.)
[39] Kvick Å 2017 X-Ray Diffraction, Materials Science Applications *Encyclopedia of Spectroscopy and Spectrometry* pp 648–55
[40] Bestimmung A, Klasse M, Klasse M, Dokument D, Copyright D, Nutzer A, Nutzung D, Digizeitschriften C and Email G 1918 Nutzungsbedingungen
[41] Wilson A J C 1978 Palouse_StableIsotopes_SedFingerprinting_2003.pdf 102–13
[42] Birks L S and Friedman H 1946 Particle size determination from x-ray line broadening *Journal of Applied Physics* **17** 687–92
[43] Wertheim G K, Butler M A, West K W and Buchanan D N E 1974 Determination of the Gaussian and Lorentzian content of experimental line shapes *Review of Scientific Instruments* **45** 1369–71
[44] Telling R H, Pickard C J, Payne M C and Field J E 2000 Theoretical Strength and Cleavage of Diamond
[45] Jimenez C M, Knezevic N Z, Rubio Y G, Szunerits S, Boukherroub R, Teodorescu F, Croissant J G, Hocine O, Seric M, Raehm L, Stojanovic V, Aggad D, Maynadier M, Garcia M, Gary-Bobo M and Durand J O 2016 Nanodiamond-PMO for two-photon PDT and drug delivery *Journal of Materials Chemistry B* **4** 5803–8
[46] Gismondi A, Reina G, Orlanducci S, Mizzoni F, Gay S, Terranova M L and Canini A 2015 Nanodiamonds coupled with plant bioactive metabolites: A nanotech approach for cancer therapy *Biomaterials* **38** 22–35
[47] Wan H, Williams R, Doherty P and Williams D F 1994 A study of the reproducibility of the MTT test *Journal of Materials Science: Materials in Medicine* **5** 154–9
[48] Schrand A M, Huang H, Carlson C, Schlager J J, Osawa E, Hussain S M and Dai L 2007 Are diamond nanoparticles cytotoxic? *Journal of Physical Chemistry B* **111** 2–7

[49] Eldawud R, Reitzig M, Opitz J, Rojansakul Y, Jiang W, Nangia S and Dinu C Z 2016 Combinatorial approaches to evaluate nanodiamond uptake and induced cellular fate *Nanotechnology* **27** 85107

[50] Chatterjee A, Perevedentseva E, Jani M, Cheng C-Y, Ye Y-S, Chung P-H and Cheng C-L 2014 Antibacterial effect of ultrafine nanodiamond against gram-negative bacteria Escherichia coli *Journal of Biomedical Optics* **20** 051014

[51] Woodhams B, Ansel-Bollepalli L, Surmacki J, Knowles H, Maggini L, De Volder M, Atatüre M and Bohndiek S 2018 Graphitic and oxidised high pressure high temperature (HPHT) nanodiamonds induce differential biological responses in breast cancer cell lines *Nanoscale* **10** 12169–79

Figures

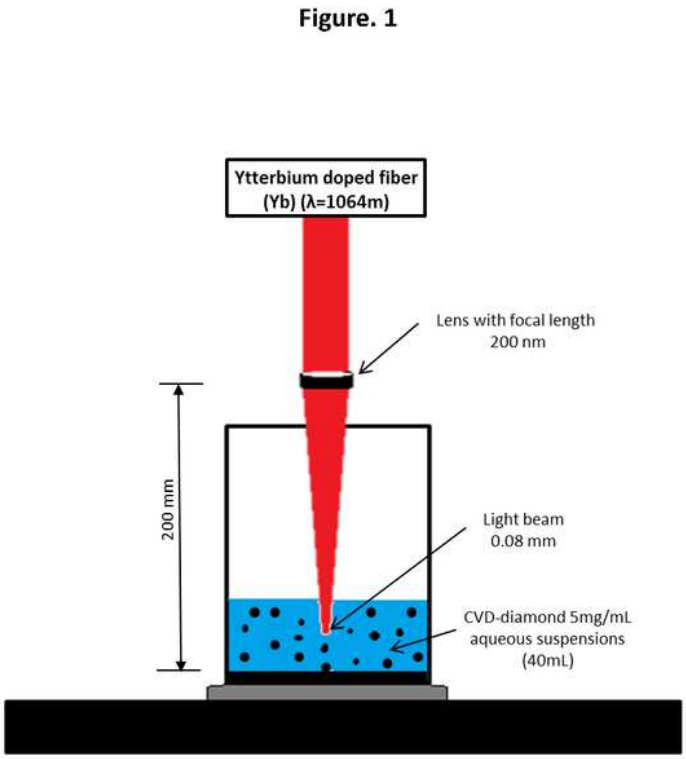

Figure 1

Draft pulsed laser ablation of ytterbium doped fiber (Yb) (Î»=1064nm) PRO Marking (Pulsed Fiber-Yb laser)

Figure. 2

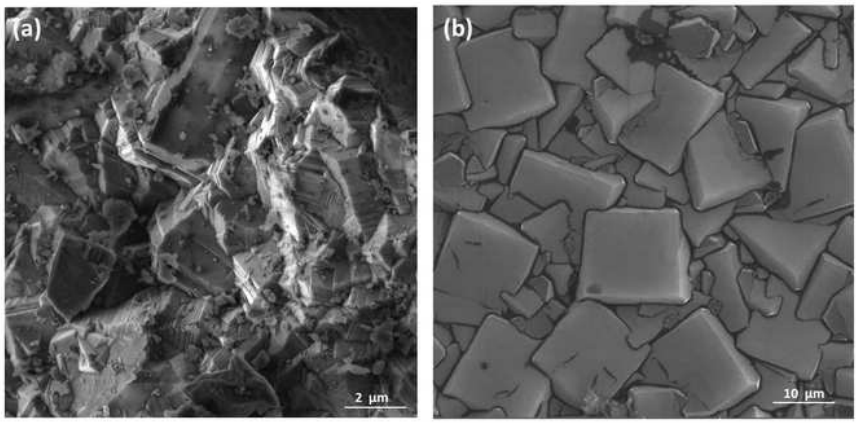

Figure 2

Sample surface in CVD Diamond before laser ablation (a) magnification of (100 kx); (b) magnification of (500 kx)

Figure. 3

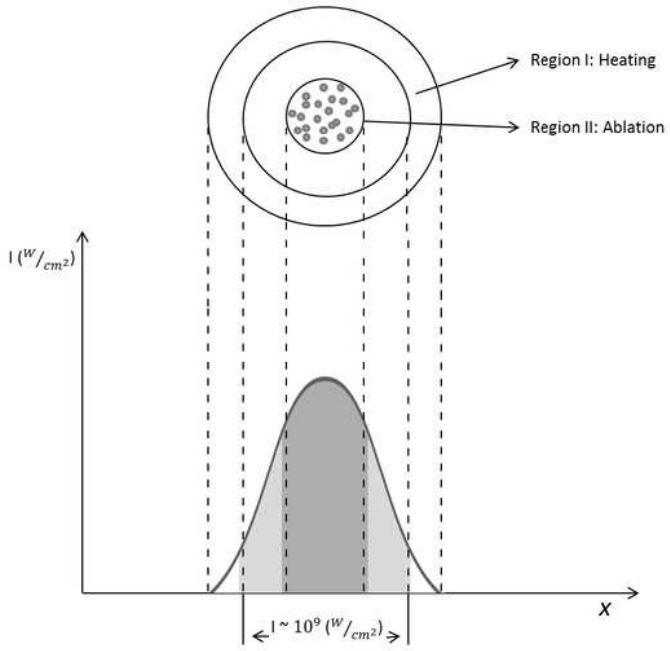

Figure 3

Schematic representation of irradiance (w / a) as a function of beam diameter.

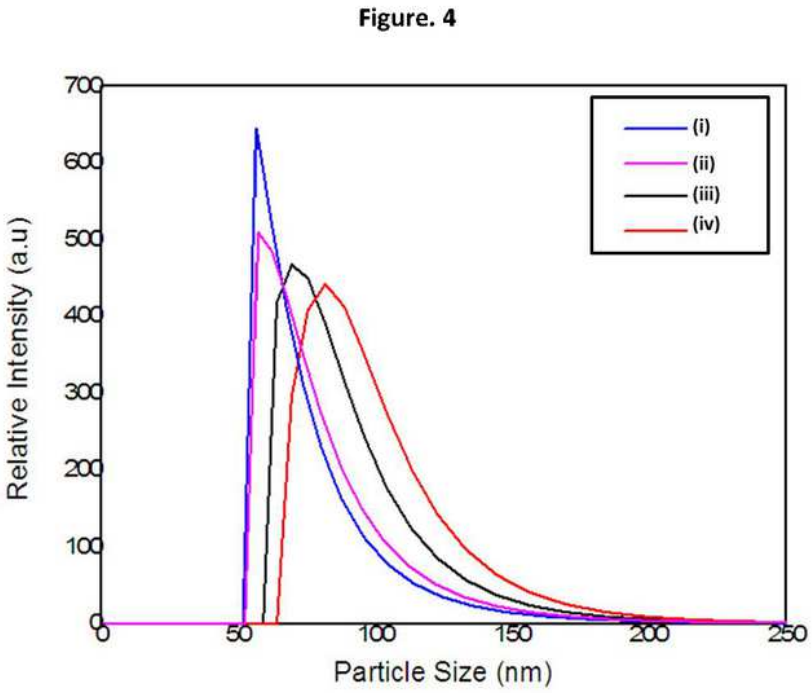

Figure 4

Particle size distribution of the (a) 60 min laser ablation and 60 min centrifugation, (b) 30 min laser ablation and 60 min centrifugation (c) 60 min laser ablation (d) 30 min laser ablation without the centrifugation process

Figure. 5

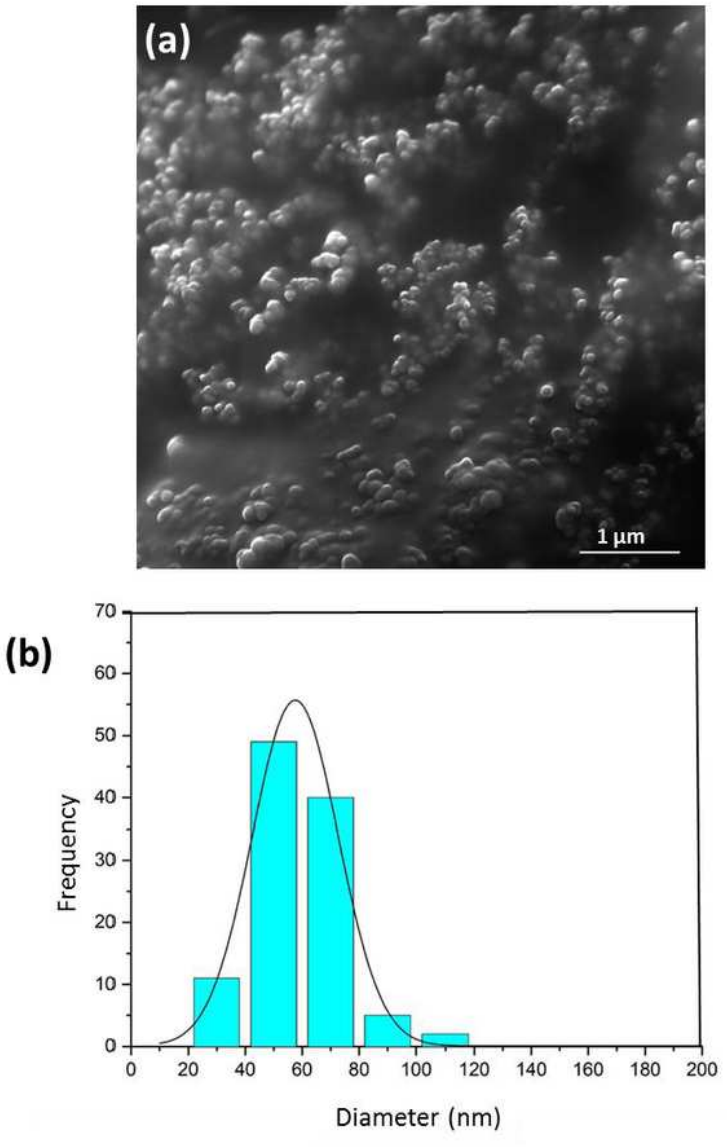

Figure 5

SEM images of the particles (a) Sample after 60 min of laser ablation, 60 min centrifugation and purification (increase of 500kx) and (b) Image distribution of particle sizes, with average size of 50,62 Â± 14,28 nm

Figure. 6

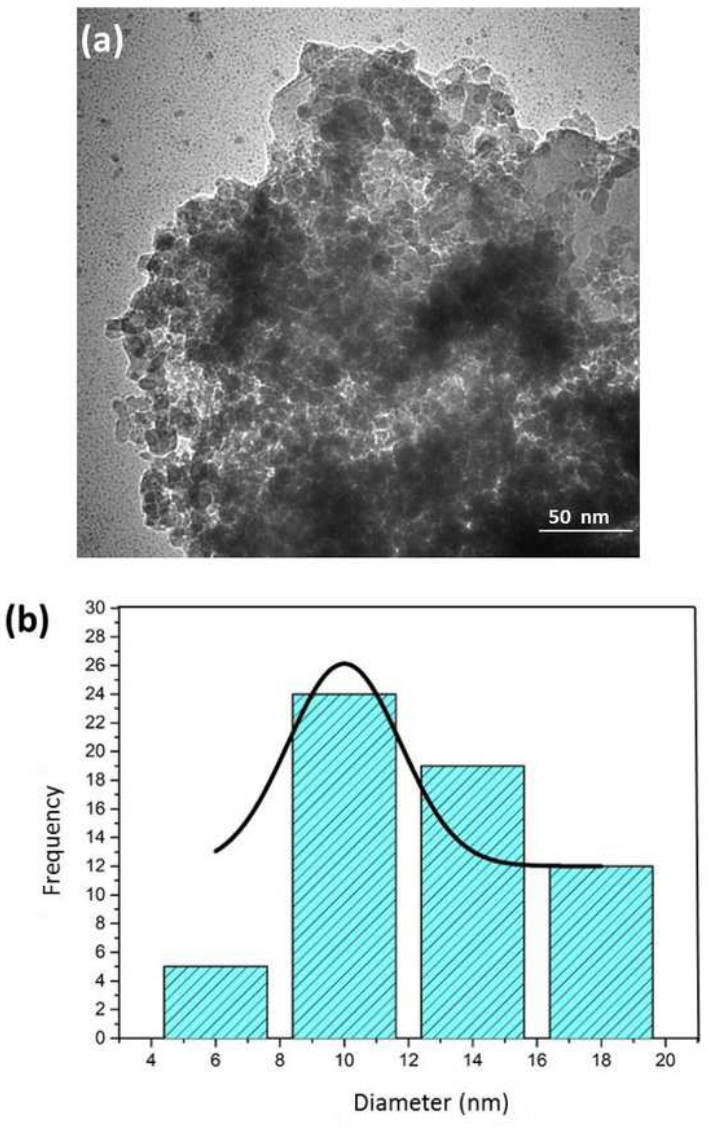

Figure 6

TEM images of the particles (a) Sample after 60 min of laser ablation, with 60 min centrifugation and purification (20 Kx) and (b) Image granulometric distribution, with average size of 20,50 ± 6,19 nm

Figure. 7

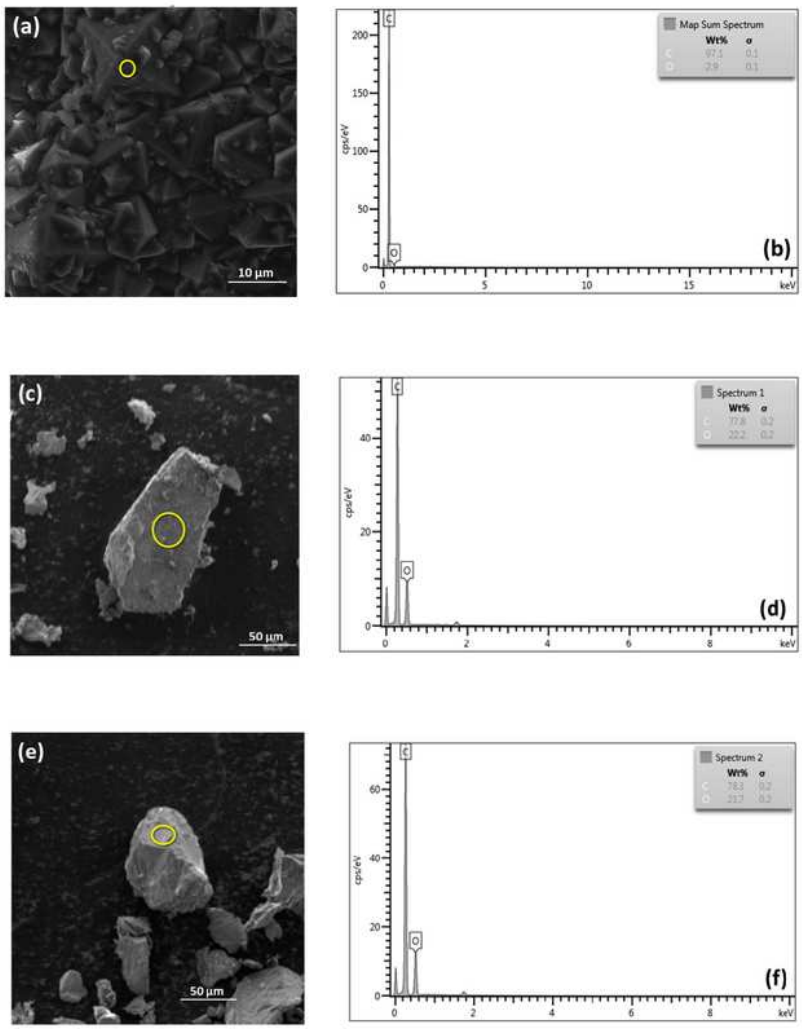

Figure 7

EDS graph (a) CVD dimond, (b) CVD-NDs (i) 30 min laser ablation and 60 min centrifugation, after acid treatment for removing SiO2 from the sample and (c) CVD-NDs (ii) 60 min laser ablation and 60 min centrifugation after acid treatment for removing SiO2 from the sample.

Figure. 8

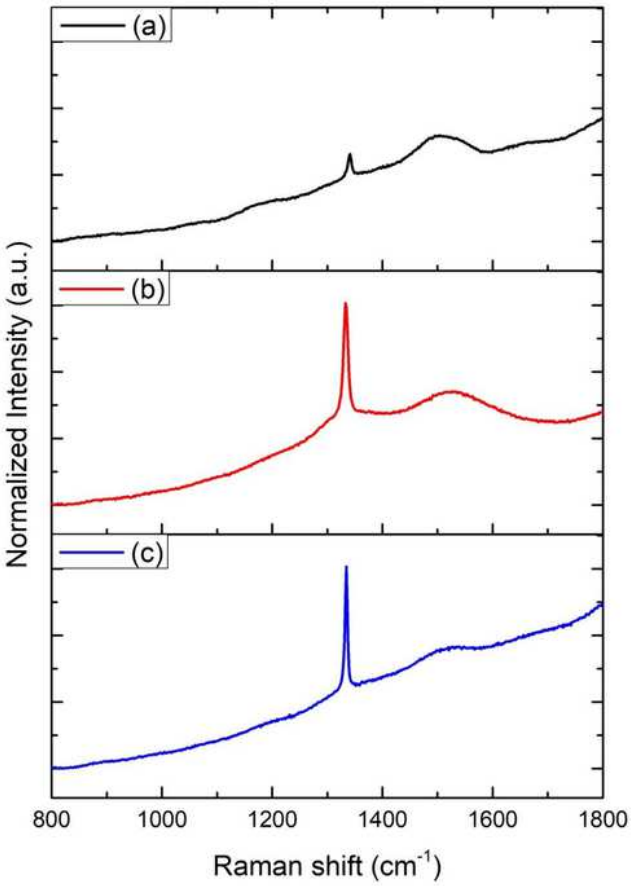

Figure 8

Raman spectra intensity (u.a) Vs of: (a) CVD diamond before laser ablation, (b) CVD-NDs (i) 30 min laser ablation and 60 min centrifugation and (c) CVD-NDs (ii) 60 min laser ablation and 60 min centrifugation

Figure. 9

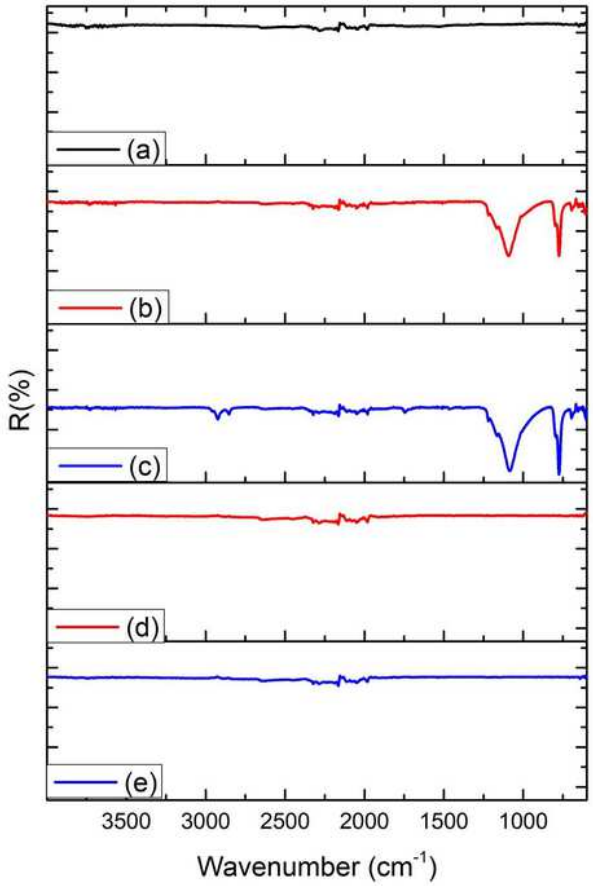

Figure 9

FTIR spectra of the: (a) CVD diamond before laser ablation, (b) CVD-DNPs (i) 30 min laser ablation and 60 min centrifugation, (c) CVD-DNPs (ii) 60 min laser ablation and 60 min centrifugation (d) CVD-DNPs (i) 30 min laser ablation and 60 min centrifugation, after acid treatment for removing SiO2 from the sample and (e) CVD-DNPs (ii) 60 min laser ablation and 60 min centrifugation after acid treatment for removing

SiO2 from the sample. The FT-IR spectrum was an average of 32 scans at a speed of 2s per scan in a range of 400-4000cm-1. The resolution of the spectrometer was of 4cm-1

Figure. 10

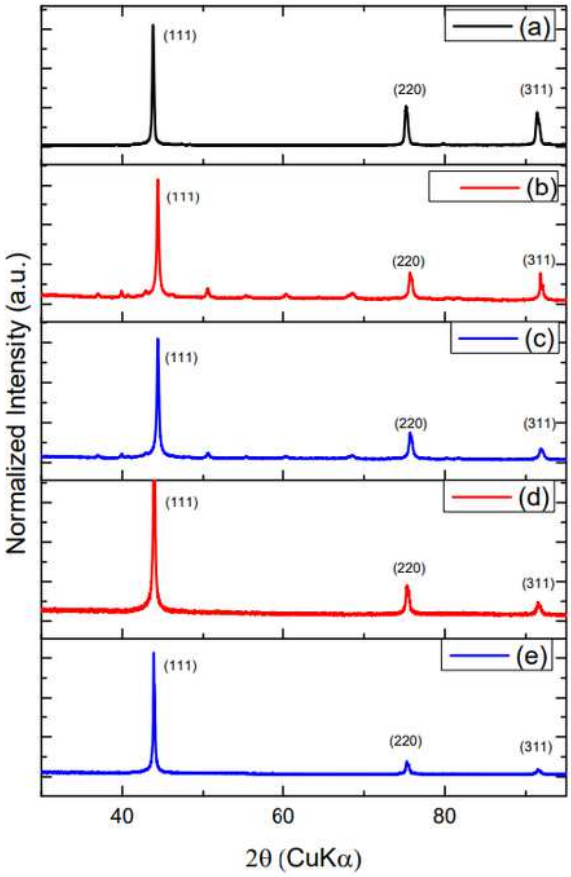

Figure 10

XRD graphics: (a) CVD diamond before laser ablation, (b) CVD-DNPs (i) 30 min laser ablation and 60 min centrifugation, (c) CVD-DNPs (ii) 60 min laser ablation and 60 min centrifugation (d) CVD-DNPs (i) 30 min laser ablation and 60 min centrifugation, after acid treatment for removing SiO2 from the sample and (e)

CVD-DNPs (ii) 60 min laser ablation and 60 min centrifugation after acid treatment for removing SiO2 from the sample

Figure. 11

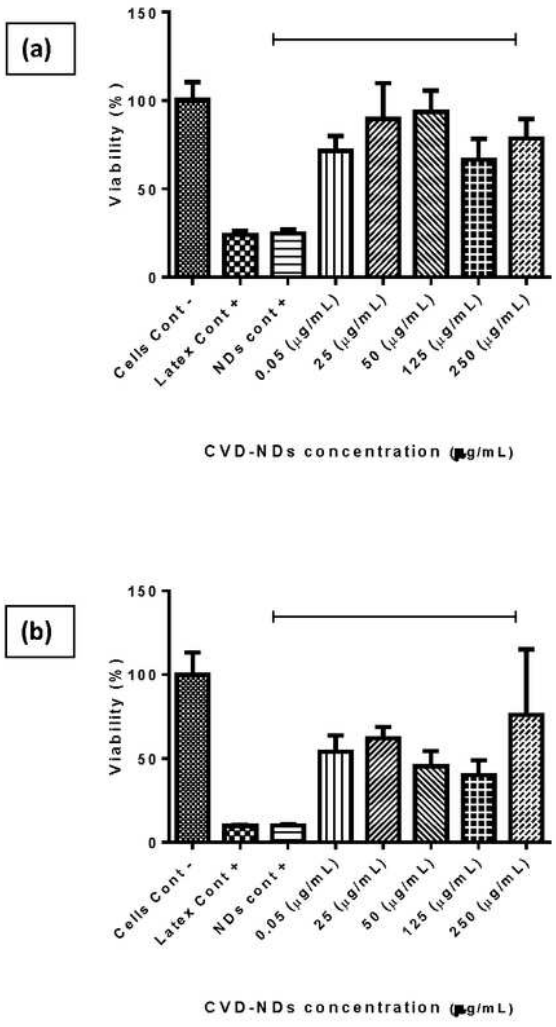

Figure 11

B16 F10 murine metastatic melanoma cells viability assessed by MTT assay in cells cultivated for 24h and 48h with CVD-NDs produced by laser ablation technique (a-b) at 5 different concentrations. The results are presented as average ± standard error for n = 5 (One Way ANOVA test and Tukey multiple

comparisons). Incubation of CVD-NDs without cells followed by the incubation with MTT and measurement of absorbance was performed in order to evaluate possible interfering signals from CVD-NDs (CVD-NDs control).

Supplementary Files

This is a list of supplementary files associated with this preprint. Click to download.

- TABLE.pdf